Supplementary Information

Absence of superconductivity in bulk $Nd_{1-x}Sr_xNiO_2$

Qing Li[#], Chengping He[#], Jin Si, Xiyu Zhu[*], Yue Zhang, Hai-Hu Wen[*]

National Laboratory of Solid State Microstructures and Department of Physics, Center for Superconducting Physics and Materials, Collaborative Innovation Center for Advanced Microstructures, Nanjing University, Nanjing 210093, China

Supplementary Table 1 | The detailed crystallographic of Rietveld refinements on $Nd_{0.8}Sr_{0.2}NiO_2$ and $Nd_{0.6}Sr_{0.4}NiO_2$ samples.

Chemical formula	$Nd_{0.8}Sr_{0.2}NiO_2$	**R_{wp}(%)**	4.16
Crystal system	Tetragonal	**R_p(%)**	3.30
Space group	P4/mmm (No. 123)	**GOF**	1.28
Density (calculated)	7.278 g/cm^3	**Wt%-Rietveld**	84.75(7)

Atom	***x***	***y***	***z***	**Occupancy**	**B_{eq}**
Nd	0.5	0.5	0.5	0.8	0.615(6)
Ni	0	0	0	0.99(8)	0.205(1)
O	0.5	0	0	1	0.252(8)
Sr	0.5	0.5	0.5	0.2	0.137(4)

Chemical formula	$Nd_{0.6}Sr_{0.4}NiO_2$	**R_{wp}(%)**	4.37
Crystal system	Tetragonal	**R_p(%)**	3.38
Space group	P4/mmm (No. 123)	**GOF**	1.09
Density (calculated)	6.908 g/cm^3	**Wt%-Rietveld**	82.99(4)

Atom	***x***	***y***	***z***	**Occupancy**	**B_{eq}**
Nd	0.5	0.5	0.5	0.6	0.300(4)
Ni	0	0	0	0.95(9)	0.647(9)
O	0.5	0	0	1	0.246(8)
Sr	0.5	0.5	0.5	0.4	0.097(3)

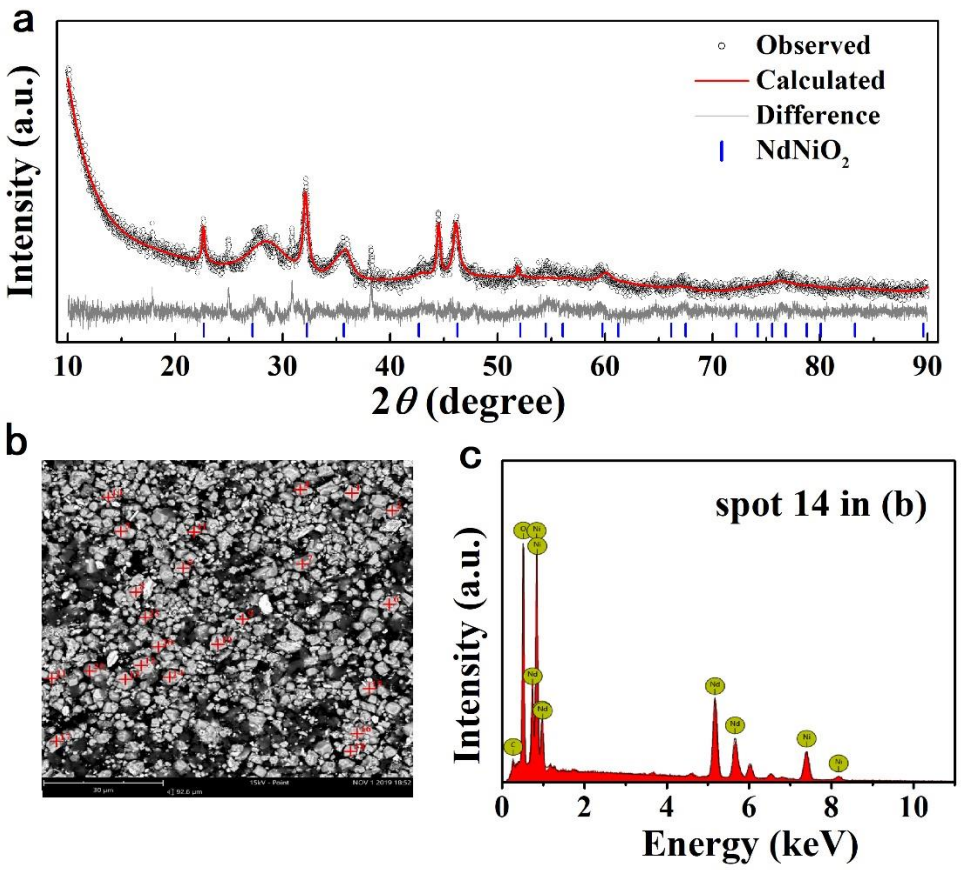

Supplementary Figure 1 | The Powder X-ray diffraction patterns, SEM image and typical energy dispersive spectroscopy of undoped $NdNiO_2$ sample. **a** The Rietveld refinements analyses show the formation of infinite-layer 112 phase. **b, c** The typical EDS pattern of spot 14 (red cross in (b)) confirms the existence of $NdNiO_2$. And the average occupied ratio of nickel in the NiO_2 plane of undoped $NdNiO_2$ is 0.91.

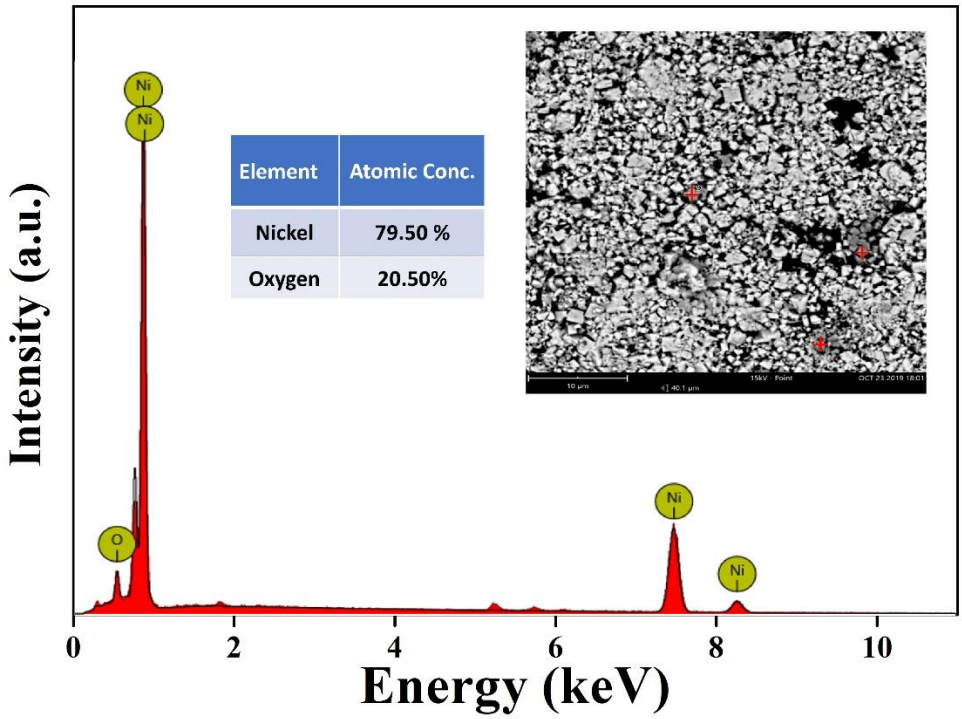

Supplementary Figure 2 | The typical EDS pattern of the dark grey area in $Nd_{0.8}Sr_{0.2}NiO_3$ samples. The energy dispersive X-ray spectroscopy is taken at the red cross of the inset image. The result shows the presence of Ni in our samples.

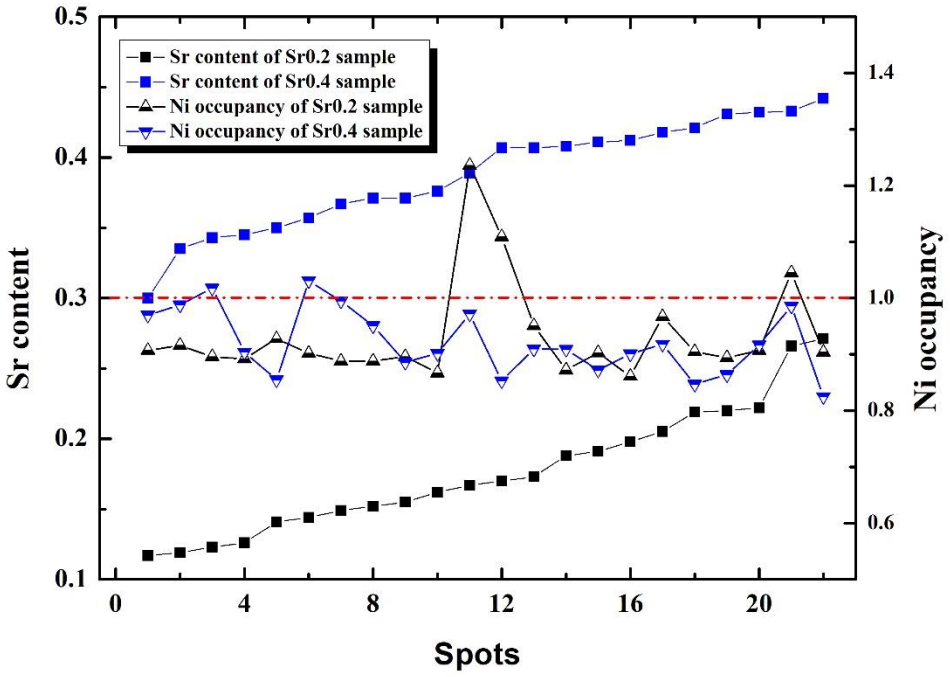

Supplementary Figure 3 | The relationship between the distributions of Sr and Ni occupancy in different grains of $Nd_{0.8}Sr_{0.2}NiO_2$ and $Nd_{0.6}Sr_{0.4}NiO_2$ samples. For the individual spots with very high Ni content like spots 11, 12, the data is likely to be affected by the nearby Ni clusters.

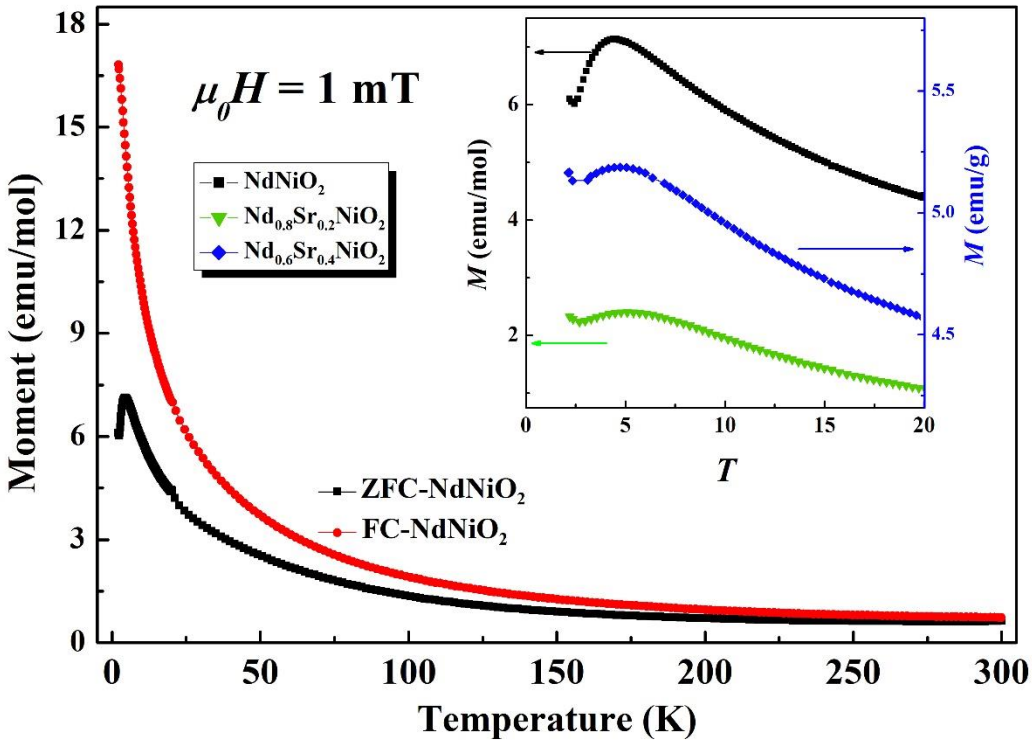

Supplementary Figure 4 | Magnetic properties of $Nd_{1-x}Sr_xNiO_2$ (x = 0, 0.2, 0.4) at low field ($\mu_0 H$ = 1 mT). Temperature dependence of magnetic moment of $NdNiO_2$ at the field of 10 Oe measured in zero field cooling (ZFC) mode and field cooling (FC) mode. Inset shows the magnetic moment versus temperature of $Nd_{1-x}Sr_xNiO_2$ (x = 0, 0.2, 0.4) samples with an external field $\mu_0 H$ = 1 mT in low temperature region with ZFC mode. An obvious irreversibility between the ZFC and FC plots and a maximum magnetization at about 5 K in the ZFC curve are observed.

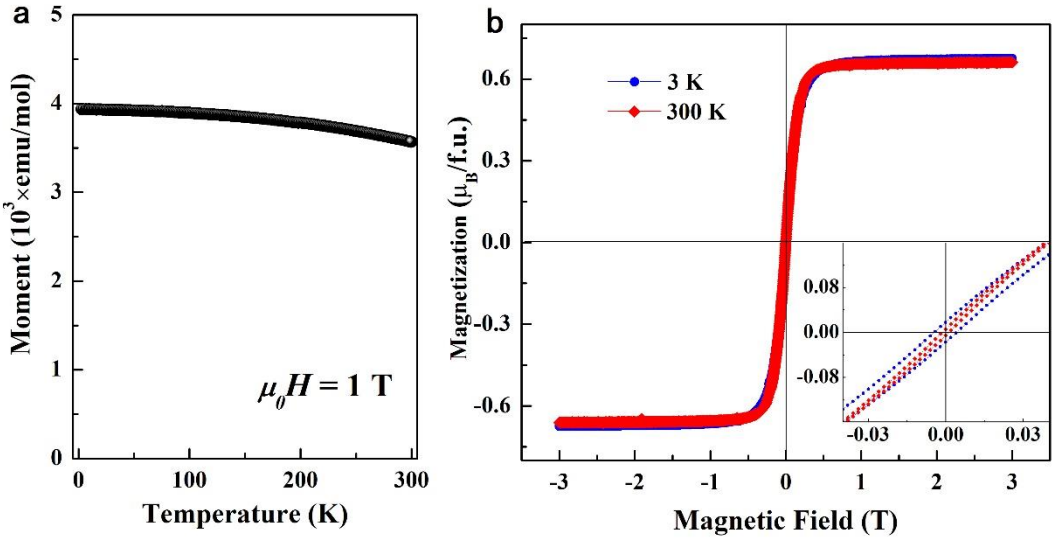

Supplementary Figure 5 | Magnetic moment versus temperature curve and magnetization hysteresis (*M-H*) loops of pure nickel. **a** Temperature dependent magnetic moment of pure nickel at the external magnetic field $\mu_0 H$ = 1 mT. **b** *M-H* curves of pure nickel at different temperatures with external magnetic fields up to ± 3 T. Inset shows the enlarged view of the M-H curves of nickel at low magnetic field.

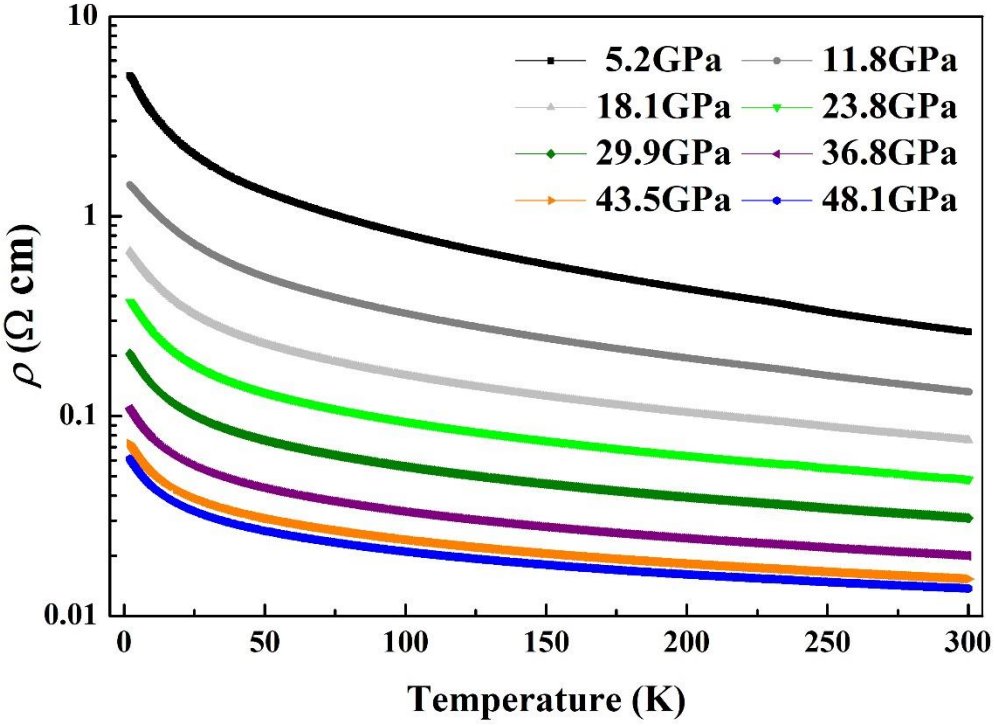

Supplementary Figure 6 | Temperature dependent resistivity of $Nd_{0.6}Sr_{0.4}NiO_2$ under pressures. The ρ_{2K}/ρ_{300K} of $Nd_{0.6}Sr_{0.4}NiO_2$ sample is about 20 with the external pressure of 5.2 GPa. With increasing pressure, the magnitude of ρ_{2K}/ρ_{300K} decreases progressively. At the highest pressure of 48.1 GPa, the value of ρ_{2K}/ρ_{300K} has dropped to 4.5, however the ρ (T) curve still exhibits a semiconducting-like feature in the whole temperature region.

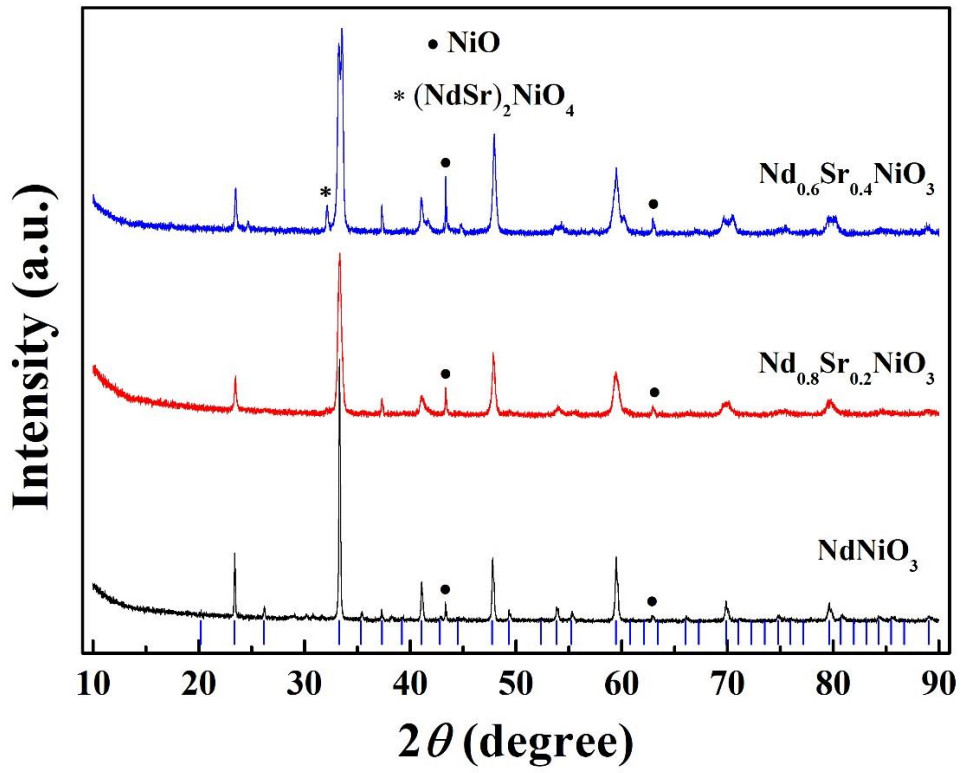

Supplementary Figure 7 | The X-ray diffraction patterns of $Nd_{1-x}Sr_xNiO_3$ (x =0, 0.2, 0.4) powders. All three samples contain small amount of NiO impurities marked with black dot (•), and one peak marked with asterisk (∗) in $Nd_{0.6}Sr_{0.4}NiO_3$ may come from the Sr-doped Nd_2NiO_4 phase.

Supplementary Note 1: Phase fraction analysis of nickel impurity and $Nd_{1-x}Sr_xNiO_2$ in present samples

In our EDS measurement, we present an evident nickel deficiency of about 5-9%. Meanwhile, we observe a large quantity of ferromagnetic nickel metal in Rietveld refinement from our XRD data. There may be a correlation between nickel impurity and nickel deficiency in $Nd_{1-x}Sr_xNiO_2$ samples, as the starting ratios of Ni:Nd:Sr in $Nd_{1-x}Sr_xNiO_2$ are stoichiometric.

As shown in Supplementary Table 1, The concentration determined from XRD is larger than the observed nickel deficiency in EDS measurement (about 5-9%). The reason for the difference may be explained by the different crystallinity, different grain size as well as the preferred orientation between Ni cluster and grains of $Nd_{1-x}Sr_xNiO_2$, the diffraction peaks of Ni is sharper than that of the latter, thus the compositional ratio between the two components from XRD may not precisely tell the true value. The concentration of nickel impurity is needed to be fixed. Therefore, the difference between nickel metal concentration in Rietveld refinement from XRD data and the observed nickel deficiency in EDS measurement is understandable.

Supplementary Note 2: The magnetic properties of pure nickel at different fields and temperatures and the Curie-Weiss fitting of effective magnetic moment in $Nd_{1-x}Sr_xNiO_2$ (x = 0.2, 0.4) samples.

As reported previously [S1-S3], the nickel undergoes a transition from paramagnetism to ferromagnetism at about 610 K - 650 K. And the average

saturated magnetic moment at low temperature (below 300 K) is about 0.6 μ_B /atom. We also measure the magnetization behavior of nickel at low temperature (see Supplementary Figure 5), a typical ferromagnetic hysteresis loop with a saturation field about 1 T can be seen.

The Curie-Weiss law is used to fit the paramagnetic term of $Nd_{0.8}Sr_{0.2}NiO_2$ and $Nd_{0.6}Sr_{0.4}NiO_2$ samples in the temperature region below 40 K by the equation: $\chi = \chi_0 + \frac{C}{T+T_\theta}$, where T_θ, χ_0, and *C* can be derived from the fitting parameters. By using the formula $C = \mu_0\mu_{\text{eff}}^2/3k_B$, one can derive the local magnetic moment μ_{eff}. We obtain the fitting results of $Nd_{0.8}Sr_{0.2}NiO_2$ (χ_0 = 7.11×10^{-3} emu·mol^{-1}Oe^{-1}, T_θ = 4.4 K, and *C* = 0.674 emu·K·mol^{-1}Oe^{-1}) and $Nd_{0.6}Sr_{0.4}NiO_2$ (χ_0 = 7.29×10^{-3} emu·mol^{-1}Oe^{-1}, T_θ = 5.2 K, and *C* = 0.517 emu·K·mol^{-1}Oe^{-1}) samples. The fitting yields the effective magnetic moments μ_{eff} of about 2.32 μ_B/f.u. for $Nd_{0.8}Sr_{0.2}NiO_2$ and 2.03 μ_B/f.u. for $Nd_{0.6}Sr_{0.4}NiO_2$ samples, respectively.

Supplementary Note 3: XRD characterization of perovskite $Nd_{1-x}Sr_xNiO_3$ (x = 0, 0.2, 0.4) samples

The as-prepared $Nd_{1-x}Sr_xNiO_3$ polycrystalline samples are crushed, ground, washed by distilled water and dried. Then, the XRD patterns are measured at room temperature, as shown in Supplementary Figure 7. We can see that the perovskite 113 phase is well formed. The rather clean XRD data indicates the high quality of the samples. Two tiny peaks which cannot be indexed with Nd_{1-}

$_{x}Sr_{x}NiO_{3}$ come from the small amount of unreacted NiO. Besides, the higher Sr-doped concentration would bring in unreacted $Nd_{2-2x}Sr_{2x}NiO_{4}$ phase in the 113 phase, as shown in the top panel of Supplementary Figure 7.

Reference

S1. Jordan, L. & Swanger, W. H. The properties of pure nickel. *Bur. Standards J. Research* **5** (6), 1291-1307 (1930).

S2. Arajs, S. & Colvin, R. V. Paramagnetism of Polycrystalline nickel. *J. Phys. Chem. Solids* **24**, 1233-1237 (1963).

S3. Billas, Isabelle M.L., Châtelain, A. & Heer , Walt A. de. Magnetism from the Atom to the Bulk in Iron, Cobalt, and Nickel Clusters. *Science* **265**, 1682-1684 (1994).